Author(s): Martin, Floran & Singh, Deepak & Belahcen, Anouar & Rasilo, Paavo & Arkkio, Antero

Title: Analytical Model for magnetic Anisotropy Dedicated to Non-Oriented Steel Sheets

Year: 2015

Version: Pre-print

Please cite the original version:

Martin, Floran & Singh, Deepak & Belahcen, Anouar & Rasilo, Paavo & Arkkio, Antero. 2015. Analytical Model for magnetic Anisotropy Dedicated to Non-Oriented Steel Sheets. COMPEL. Volume 34, Issue 5. 6. DOI: 10.1108/COMPEL-02-2015-0076.

Analytical Model for Magnetic Anisotropy of Non-Oriented Steel Sheets

Floran Martin, Deepak Singh, Anouar Belahcen, Paavo Rasilo, Ari Haavisto, and Antero Arkkio
Aalto University, Departement of Electrical Engineering and Automation, Otakaari 5, 02150 Espoo, Finland

Abstract— Recent investigations on magnetic properties of Non-Oriented steel sheets enhance the comprehension of the magnetic anisotropy behaviour of widely employed electrical sheets. Our investigation consists of developing an analytical model to consider these magnetic properties while modelling electromagnetic systems. From rotational measurements, the anhysteretic curves are interpolated in order to extract the magnetic energy density for different directions and amplitudes of the magnetic flux density. Furthermore, the analytical representation of this energy is suggested based on statistical distribution which aims to minimize the intrinsic energy of the material. Our model is validated by comparing measured and computed values of the magnetic field strength. Finally, it is implemented into a finite element method.

1. Introduction

Non-oriented (NO) electrical steel sheets are usually composed of iron doped with silicon. Although their manufacturing process tends to confer isotropic properties (Kedous-Lebouc 2006, Rasilo et al. 2011), magnetic anisotropy has been always observed and recently investigated (Chwastek 2013, Handgruber et al. 2014, Higuchi et al. 2014). Three main intrinsic phenomena involve anisotropic characterization of body centred cubic iron (Chikazumi 1997):

- Shape anisotropy is a purely magnetostatic phenomenon. It depends on the shape of ferromagnetic crystal and its magnetic moment. These magnetic moments within the crystal produce not only an external magnetic field but also an internal field known as the demagnetization field (Osborn 1945).
- Magnetocrystalline anisotropy is mainly caused by spin-orbit interaction (Cullity and Graham 2008). Thus it depends on the molecular structure of the crystal. In grain-oriented (GO) electrical steel sheet, the body centred cubic structure for pure iron is enhanced in order to bring a hard direction in the diagonal of the cube. With NO steel sheet, this phenomenon is diminished.
- Magnetostriction results by strain due to an external field which rotates magnetic moments interaction (Cullity and Graham 2008). Although, this effect would be neglected in case of perfectly spheroidal crystal, the spin- orbit interaction also involves significant magnetomechanical effects on electrical sheets (vibration, additional losses, etc.) (Belahcen et al. 2014, Cullity and Graham 2008, Fujisaki et al. 2004, Skomski 2008).

Models of magnetic anisotropy derive from different formulations regarding to the target application. The following non-exhaustive literature review considers applications dedicated to finite element formulation. Since the magnetic anisotropy infers a dependence of reluctivity on both amplitude and direction of the applied flux density, its model can be developed by interpolating between two adjacent measured **B-H** curves (Shirkoohi and Liu 1994). Under rotational applied flux density, Enokizono and Soda (1995) develop a Garlerkin's formulation based on the decomposition of the magnetic field into a purely rotational field (isotropic) and an effective field (anisotropic). The isotropic reluctivity and components of the effective magnetic field are interpolated and implemented into their numerical method.

Derived from magnetocrystalline theory (Skomski 2008), Vernescu-Spornic et al. (2000) develop a mixed Preisach/biastroide model. The biaxial anisotropy is considered by minimizing the sum of the applied field and the magnetocrystalline anisotropy energy, which depends on the first anisotropy constant. Their model was validated by comparison with measurements on NiFe samples at 1.5 T and 50 Hz under rotating induction, alternating sinusoidal along hard direction and both rolling and

transverse directions. However discrepancies were noticed at low flux level especially under rotational measurements. Considering the phase mode theory (Néel 1944), Fiorillo et al. (2002) investigate the impact of experimental setup on magnetic measurements of GO iron steel sheets under alternating flux. Their improved model includes not only the first and the second anisotropy constants but also hysteresis loops. From 0.4 to 1.5 T, their model fits well with measurements performed on X-stack (low effect of shape anisotropy), Epstein frame and Single Sheet Tester.

Based on energy/coenergy density principle (Silvester and Gupta 1991), Péra et al (1993a), (1993b) expand a phenomenological model on GO sheets which needs only the rolling (RD) and the transverse (TD) direction given by manufacturers. For low value of coenergy density (shape anisotropy), hard direction is close to 90° while the hard direction appears, in theory, in the diagonal of a cubic crystal (55°) for higher coenergy density level. Although, their computational implementation requires some numerical derivation based on interpolation, their model matches with alternating flux measurements for 4 various directions in the range of 200 A/m to 30 kA/m. However, the four magnetization modes introduced by Néel (1944) are not fully described by this phenomenological approach, so data in more directions are needed to characterize these sheets completely (Higuchi et al. 2014, Meunier 2008). Thus, Higuchi et al. (2014) model the magnetic energy density for NO sheets with Fourier series. Their decomposition is based on alternating flux with 7 different cutting angles on Single Sheet Tester (Higuchi et al. 2012). Their approach shows that magnetic anisotropy impacts on torque ripples and hysteresis losses of an interior permanent magnet motor.

Mainly, the magnetic anisotropy can be modelled with at least one of those three approaches. The first one, based on interpolation with piecewise polynomial functions, should grant the best accuracy but it would also require the most computational effort and a large amount of measurements. The second one, based on material theory, should present a relatively good accuracy depending on the assumptions. For instance, the magnetostrive phenomenon and the magneto-mechanical impact on the magnetic behaviour are usually neglected. Moreover, those models are usually developed such as the magnetization is expressed as a function of the magnetic field strength. Thus, those non-linear models would require an inversion process for implementation in finite element methods with magnetic vector potential. The third approach should present a relatively correct accuracy since the components of magnetic flux density are determined by differentiation of the energy density. Since the energy density is a scalar, its representation with piecewise polynomial functions would reduce the computational effort compared to an interpolation of every components of the magnetic field.

In this paper, we present an original model developed by including Gumbel distribution on energy density principle. Originally, Gumbel distribution can be employed to model the distribution of the maximum (or the minimum) in many samples characterized with various distributions (Gumbel 1935). The arrangement of the grains, containing different crystals within the sheets, depends on manufacturing process. Grain size, wall thickness, and magnetic moment orientation differ within the NO sheets. While applying an external field, we assume that this macroscopic structure will move in order to minimize its intrinsic energy. As energy density is a scalar, its implementation in finite element method should result in faster resolution of the energy functional formulation than manipulating **B** and **H** vectors. Whereas the energy density presents an implicit form in (Bíró et al. 2010, Péra et al. 1993a), we suggest an explicit formulation in order to ease the computations. The proposed model is fitted with 16 parameters from 9 rotational measurements with Gumbel functions. Finally, the suggested model is implemented into a 2D finite element method.

2. Extraction of energy density from rotational measurements

Measurements have been carried out in two cross shape NO sheets (Belkasim 2008). In order to reduce the effect of shape anisotropy (Fiorillo et al. 2002), the rolling direction of both sheets is shifted by 180° . Every component of **B**-**H** loci are measured with 3 072 points at 10 Hz. Rotating

magnetic flux density presents 9 different amplitudes: 0.2 T, 0.42 T, 0.64 T, 0.87 T, 1.09 T, 1.34 T, 1.52 T, 1.65 T, and 1.89 T. We are interested in extracting the anisotropic energy density which does not produce losses over a cycle.

A. Interpolation of anhysteretic curves

In order to retrieve the anhysteretic curves, we remove the magnetic losses. The overall magnetic losses p_{mag} can be determined by integration over a full period T (Rasilo et al. 2011):

$$p_{mag} = \frac{1}{T}\int_0^T \boldsymbol{H}.\left(\frac{d\boldsymbol{B}}{\mathrm{d}t}\right)dt = \frac{1}{T}\left[\int_0^T h_{x-meas}\left(\frac{db_{x-meas}}{dt}\right)dt + \int_0^T h_y\left(\frac{db_{y-meas}}{dt}\right)dt\right] \tag{1}$$

The components of the magnetic flux density b_x and b_y as well as the components of the magnetic field strength h_x and h_y can be decomposed in Fourier series:

$$\begin{aligned} b_{x-meas} &= b_{x0} + \sum_{k=1}^{+\infty} b_{xk}\cos\left(k\omega t + \phi_{xk}\right) & h_{x-meas} &= h_{x0} + \sum_{p=1}^{+\infty} h_{xp}\cos\left(p\omega t + \phi_{xp}\right) \\ b_{y-meas} &= b_{y0} + \sum_{k=1}^{+\infty} b_{yk}\sin\left(k\omega t + \phi_{yk}\right) & h_{y-meas} &= h_{y0} + \sum_{p=1}^{+\infty} h_{yp}\sin\left(p\omega t + \phi_{yp}\right) \end{aligned} \tag{2}$$

where ω is the time pulsation of the supply, ϕ is the phase shift between the harmonic and the fundamental. Indices k and p relates to the flux density and the field strength respectively. Index *meas* refers to the measured loci which include the magnetic losses. For simplicity of the calculation, we consider one harmonic of the flux density and one harmonic of the field strength.

The expression of the magnetic losses becomes:

$$p_{mag-kp} = \frac{k\omega}{2}\left[b_{xk}h_{xp}\sin\left(\phi_{xp} - \phi_{xk}\right) + b_{yk}h_{yp}\sin\left(\phi_{yp} - \phi_{yk}\right)\right] \tag{3}$$

It can be shown that the magnetic losses are non-nil only if $k = p$.

Finally, the overall magnetic losses can be removed by setting the phase shift of every harmonic of the magnetic field such as:

$$\phi_{xp} = \phi_{xk} \qquad \text{and} \qquad \phi_{yp} = \phi_{yk} \tag{4}$$

With perfectly circular **B** loci, the components b_{x-meas} and b_{y-meas} are only composed of the fundamental and so removing the magnetic losses can be performed by cancelling the phase shift of the fundamental of both h_{x-meas} and h_{y-meas}.

Since the anisotropic angle between magnetic magnitudes present less variation when the material approaches its saturation, the reference angle $\phi_{h-\max}$ corresponds to the **H** locus matching with 1.89 T **B** locus. From the 3 072 different directions, we select the amplitude of 9 **H** loci whose polar angle is closest to the reference. While each **H** amplitude is associated with its corresponding **B** amplitude, H(B) anhysteretic curves (Figure 1) are extracted and interpolated with a shape-preserving piecewise cubic polynomial function.

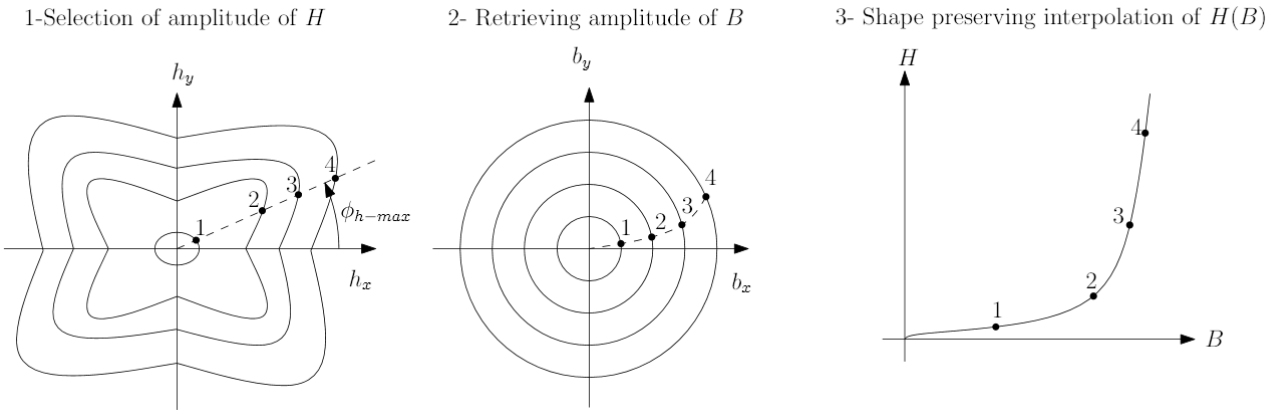

*Fig. 1. Representation of the method for determining the anhysteretic curves from **B**-**H** loci for a given direction* $\phi_{h-\max}$

B. Energy density distribution and equal contour of energy density

The energy density $w(b_x, b_y)$ is computed by integration of the interpolated anhysteretic curves by:

$$w(b_x, b_y) = \int_0^{\boldsymbol{B}} \boldsymbol{H}.d\boldsymbol{B} \tag{5}$$

Figure 2 represents the extracted energy density from the measurements by the described method.

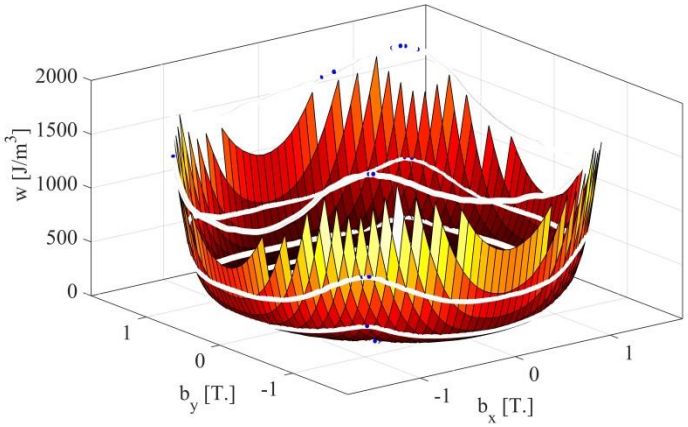

Fig. 2. Representation of the magnetic energy density $w(b_x, b_y)$ *extracted from the quasi-static measurements*

This energy density is interpolated by a surface spline in order to compute equal contour of energy density. From the 0.2 T and 1.89 T loci, the highest and the lowest energy density are respectively selected for both extrema contours of energy density. With all other loci, average values of energy density are retained in order to compute the equal contour of energy with Brent's method (Brent 1973). Since the modified elliptic model assumes that the equal contours of energy density are orthogonal to both axes (0, $\boldsymbol{b}_x$) and (0, $\boldsymbol{b}_y$), we rotate the b_x and b_y components in order to fulfil this assumption.

$$\begin{bmatrix} b_{xR} \\ b_{yR} \end{bmatrix} = \begin{bmatrix} \cos\phi_w & \sin\phi_w \\ -\sin\phi_w & \cos\phi_w \end{bmatrix} \times \begin{bmatrix} b_x \\ b_y \end{bmatrix} \tag{6}$$

From our measurements, the rotation angle ϕ_w is 3.01°. This angle can be interpreted as a misalignment between the macroscopic rolling direction and the x axis of the measurements. Figure 3 represents the equal contours of energy density.

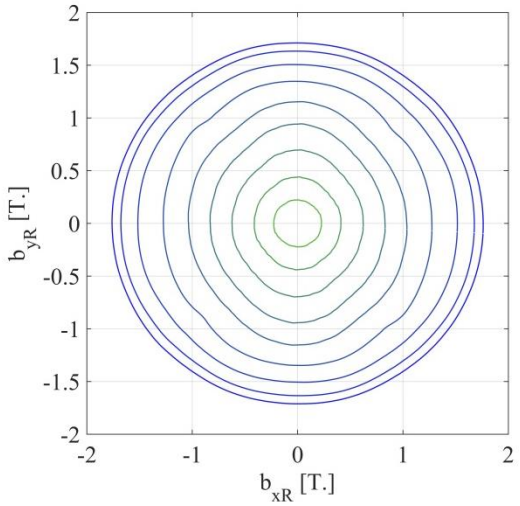

Fig. 3. Contours of equal energy corresponding to the interpolated anhysteretic curves

Since, we aim to improve the modified elliptic model of isolines of energy developed by T. Péra et al. (Bíró 2010, Péra 1993a), we compute the value of energy density w_0, the intersection B_{x0} and B_{y0} between these contours and both axes $(0,\ b_x)$ and $(0,\ b_y)$ respectively, and the parameter n which is equal to 2 in the specific case of elliptic contours (Table I).

Table I. Data of equal energy contours

w_0 [J/m^3]	B_{x0} [T]	B_{y0} [T]	n
5.13	0.225	0.222	2.000
13.35	0.410	0.439	1.855
24.53	0.622	0.695	1.808
37.93	0.829	0.942	1.792
55.16	1.035	1.153	1.772
96.47	1.274	1.347	1.931
236.85	1.516	1.506	1.976
628.05	1.677	1.634	1.992
1105.32	1.761	1.711	1.999

3. Analytical representation based on Gumbel distribution

The modified elliptic model represents the equal contour of energy density with the following assumptions (Bíró 2010, Péra 1993a):

- **B** and **H** are collinear in both rolling and transverse directions so equal contours of energy density are orthogonal to these directions;
- Hysteresis is neglected in order to provide a monotonous implicit function $H_y(H_x)$.

Thus equal contours of energy density can be modelled by the following implicit function *F*:

$$F(b_x,\ b_y)=\left(\frac{b_x}{B_{x0}}\right)^n+\left(\frac{b_y}{B_{y0}}\right)^n-1=0 \qquad (7)$$

The 3 functions B_{x0}, B_{y0} and n can also be calculated as a function of the energy density as in (Bíró 2010, Péra 1993a).

A. An improved expression of energy density

With our approach, we propose an explicit expression of the energy density in order to compute components of magnetic field by analytical differentiation. In its general form, energy density could be expressed by:

$$w\,(b_x,\ b_y) = C(b_x,\ b_y)\ b_x^{\,n(b_x,\ b_y)} + D(b_x,\ b_y)\ b_x^{\,n(b_x,\ b_y)} \tag{8}$$

where *C*, *D*, and n are 3 functions that only depend on the components of magnetic flux density.
With the suggested model, equal contours of energy density are linked with the original approach by:

$$F = \frac{C}{w_0} b_x^{\,n} + \frac{D}{w_0} b_y^{\,n} - 1 \tag{9}$$

By simple identification of (7) and (9), we can notice that functions n are the same and functions *C*, *D* can be computed by:

$$C = \frac{w_0}{B_{x0}^{\,n}} \qquad\qquad D = \frac{w_0}{B_{y0}^{\,n}} \tag{10}$$

These 3 functional parameters can be interpolated by piecewise polynomials but in order to ease the computation of energy density differentiations, we suggest an interpolation by Gumbel distributions.

B. Representation and interpolation of functional parameters

Considering NO steels, functions *C*, *D*, and n can be expressed as a function of the amplitude of magnetic flux density **B**. Originally, Gumbel distribution aims to approach the maximum value corresponding to many samples with different distributions. While applying an external field, we assume that grains and walls will move in order to minimize the intrinsic energy. Hence, functional parameters *C* and *D* could be interpolated with the inverse of a Gumbel function g. The functional parameter n which corresponds to the intrinsic magnetic moment could be modelled with a Gumbel function too. Moreover, from the extracted value of n (Table I), we can notice that the elliptic assumption would be correct in both cases: without applied field and when steel reaches its saturation. So, we suggest the following interpolated functions:

$$\begin{aligned} C(B) &= g\left(B,\ \alpha_C,\ b_C,\ \beta_C,\ k_C\right)^{-1} \\ D(B) &= g\left(B,\ \alpha_D,\ b_D,\ \beta_D,\ k_D\right)^{-1} \\ n(B) &= g\left(B,\ \alpha_D,\ b_D,\ \beta_D,\ k_D\right) + 2 \end{aligned} \tag{11}$$

where *B* is the amplitude of the magnetic flux density, α, b, β, and k are the parameters of the Gumbel distribution.
The Gumbel distribution is given by:

$$g(B) = \alpha\ \exp\left[-\frac{B-b}{\beta} - \exp\left(-\frac{B-b}{k\,\beta}\right)\right] \tag{12}$$

The functional parameters *C*, *D*, and n are represented in figures 4-6.

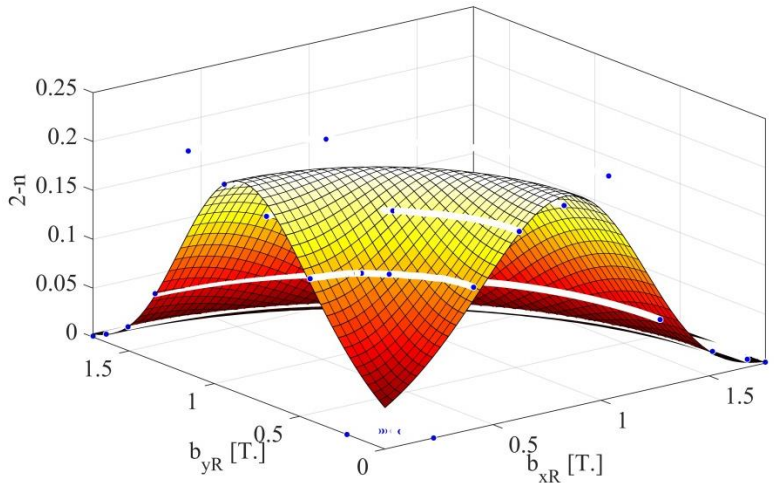

Fig. 4. Representation of the function $n(b_x,\ b_y)$ *fitted by Gumbel distribution*

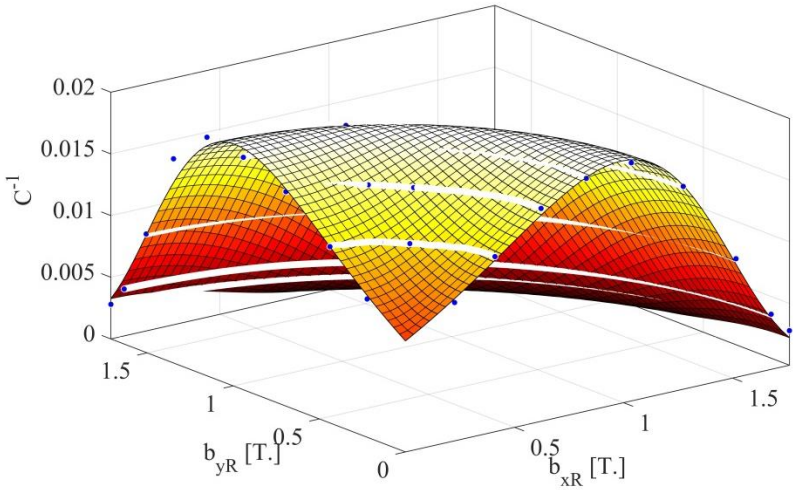

Fig. 5. Representation of the function $1/C(b_x,\ b_y)$ *fitted by Gumbel distribution*

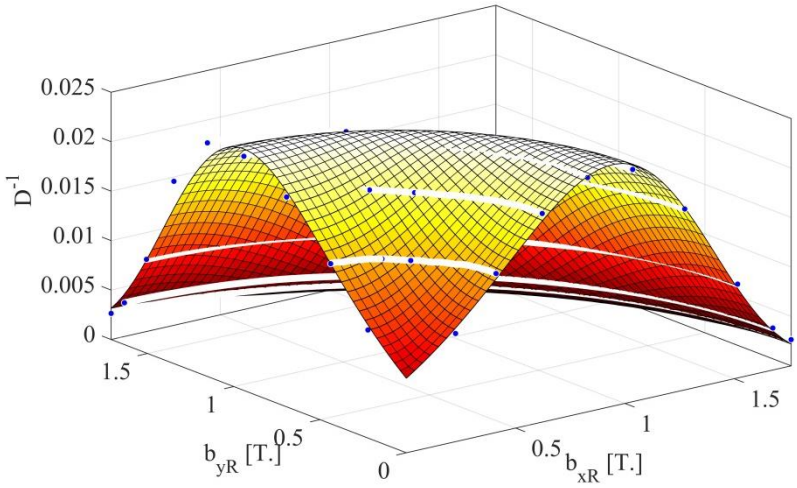

Fig. 6. Representation of the function $1/D(b_x,\ b_y)$ *fitted by Gumbel distribution*

The functional parameters are fitted with a non-linear least squares method that minimizes the absolute difference of the residuals, rather than the squared difference. The fitted parameters, error and correlation coefficients are given in table II.

Table II. Parameters of the Gumbel distributions to model n, C, and D in the energy density model

	$2-n\left(b_x,\ b_y\right)$	$C\left(b_x,\ b_y\right)^{-1}$	$D\left(b_x,\ b_y\right)^{-1}$
α	0.1149	0.0445	0.0609
b	0	1.2805	0.7288
β	-0.2114	-0.8186	-0.4040
k	3.2967	0.4604	1.4435
Correlation r^2	0.9957	0.9947	0.9941
Error *rmse*	0.0059	0.0004	0.0005

First, we can notice that Gumbel distribution provides both good correlation coefficients and small root mean square errors for the interpolation of the 3 functional parameters C, D, and n. Since we model C, D, and n to describe the energy density as a function of the amplitude of B, we suppose that equal contours of energy are close to circular shape. Hence, the suggested model would not be appropriate for material with strong anisotropic behaviour such as GO steel sheets. The parameter k which allows a modification of original slopes of Gumbel distribution has been introduced in order to improve the interpolation.

4. Investigation on the suggested model

The **H** loci can be determined by differentiating the energy density with respect to the components of flux density. These computed **H** loci are compared with the measured loci. A sensitivity analysis is introduced to evaluate the effect of uncertainty on flux density measurements.

A. Comparison between measured and computed magnetic field

Components of magnetic field strength are determined by:

$$h_x = \frac{\partial\, w\left(b_x,\ b_y\right)}{\partial\, b_x} \qquad h_y = \frac{\partial\, w\left(b_x,\ b_y\right)}{\partial\, b_y} \tag{13}$$

These components only depend on the components of magnetic flux density and parameters of Gumbel distribution. Hence, **H** loci can be computed from measured **B** loci. In Figures 7a-7i, we can notice that both measured and computed **H** loci present similar shapes. For higher value of magnetic flux density, the flower shape related to anisotropy is reproduced by the suggested model. For low value of magnetic flux density, the model reproduces a quasi-isotropic shape. Then, the average relative error between the model and the measurements is 22 %. The highest error is reached for the locus corresponding to the amplitude of 1.79 T of magnetic flux density (Figure 7i). Therefore, we propose to investigate the impact of errors in the measurements of the magnetic flux density.

B. A sensitivity analysis

In order to appreciate the comparison between computed and measured H loci, we propose to model **H** loci with an error of +/- 1.6% on the measurements of b_x and b_y. The grey area in figure 7a-7i represents the impact of this error on the computed magnetic field strength. We can notice that for 1.79 T which contains the maximum error of our proposed model, the impact of uncertainty in magnetic flux density measurements is strongly significant. Thus, it may not be relevant to estimate the accuracy of the model based on this locus.

Besides, since the **B** loci are not perfectly circular, their hysteresis angles differ within every locus. Hence, the proposed method to extract the *B-H* anhysteretic curves for different directions also presents some error. Although, errors arise from different phenomena, the proposed method models the magnetic anisotropy of non-oriented steel sheets with relatively low error (22 %).

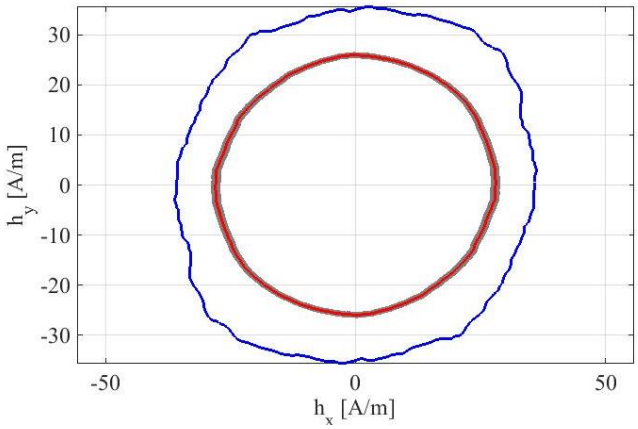

(a) **H** locus - 0.20 T

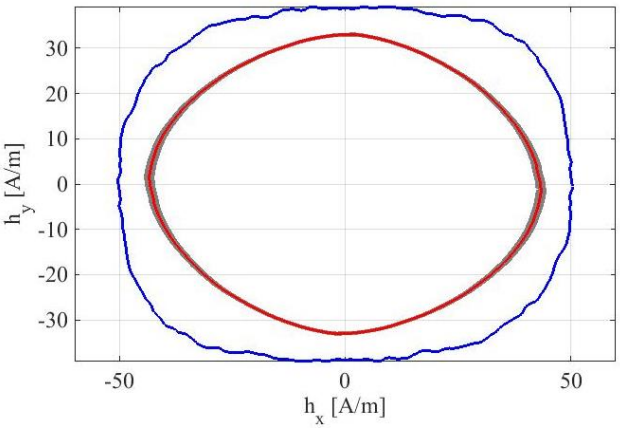

(b) **H** locus - 0.42 T

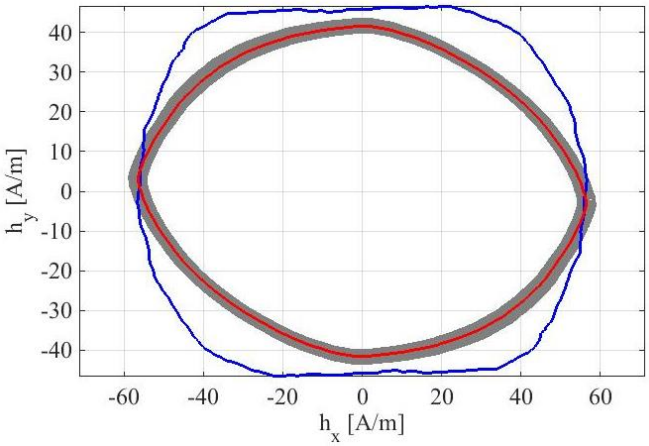

(c) **H** locus - 0.64 T

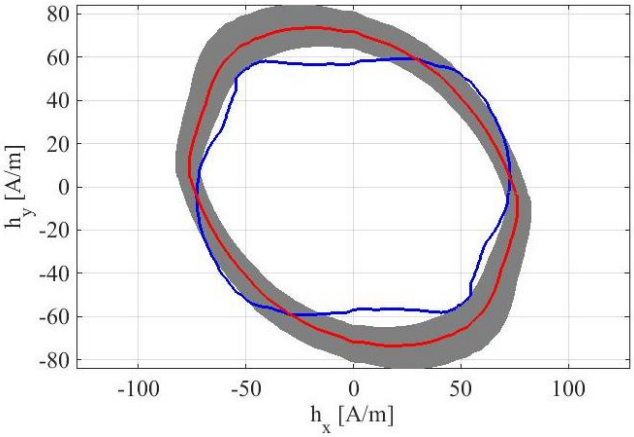

(d) **H** locus - 0.87 T

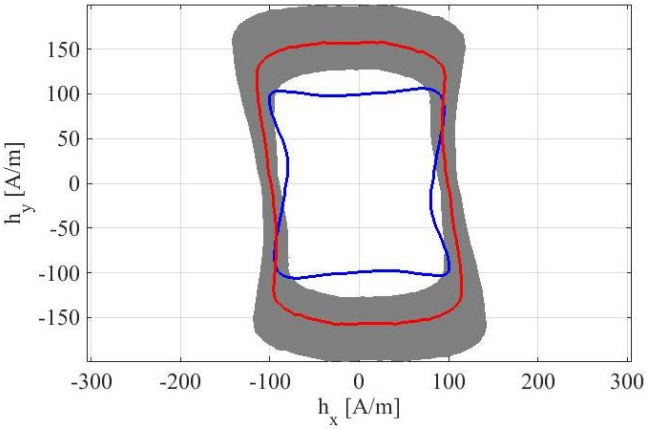

(e) **H** locus – 1.09 T

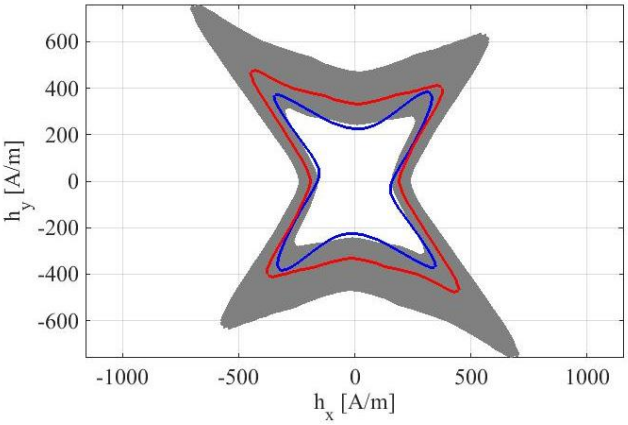

(f) **H** locus – 1.34 T

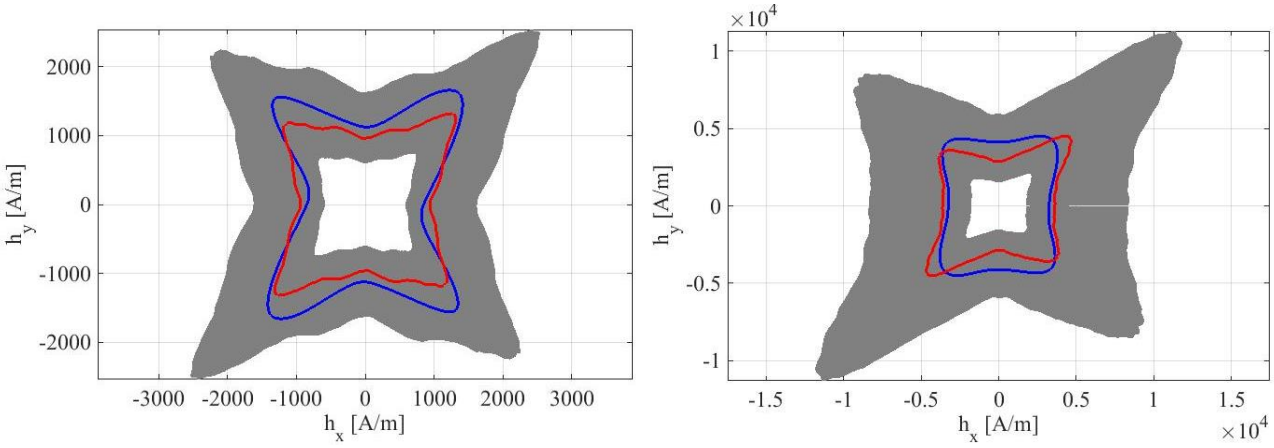

(g) **H** locus – 1.52 T (h) **H** locus – 1.65 T

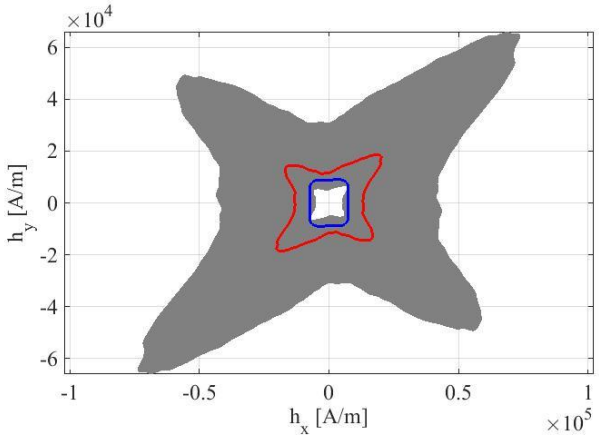

(i) **H** locus – 1.79 T

Fig. 7. Comparison of the calculated magnetic field (in red) and the measured field (in blue) from the rotating measure at 10 Hz. The grey area corresponds to the impact of +/- 1.6% of error in flux density measurements on the computed field.

5. Implementation in finite element method

In order to enhance our objective, we implement the proposed model into a 2D finite element method. The section S of a rotational single sheet tester (Figure 8a) is discretized into first order triangles and the magnetostatic problem is defined with the magnetic vector potential $\boldsymbol{A}$. The governing partial differential equation is solved with the Garlekin's method by minimizing the energy functional $\mathcal{F}$ given by (Meunier 2008):

$$\mathcal{F} = \int_S \left[\int_0^{\boldsymbol{B}} \boldsymbol{H}^T d\boldsymbol{B} - \boldsymbol{J}\boldsymbol{A} \right] dS \tag{14}$$

where $\boldsymbol{J}$ represents the current density sources.

Since the magnetic properties are anisotropic and non-linear, its minimization requires an iterative process. The estimated magnetic vector potential $\boldsymbol{A}_k$ is updated after each k iteration with the Newton-Raphson method. Its expression is given by:

$$\boldsymbol{A}_{k+1} = \boldsymbol{A}_k - \boldsymbol{P}_k^{-1} \boldsymbol{R}_k \tag{15}$$

where the residual vector $\boldsymbol{R}$ and the Jacobian matrix $\boldsymbol{P}$ are composed of the terms given by:

$$\begin{aligned} R_i &= \int_S \nabla \times \left(N_i e_z\right)^T \boldsymbol{H}\left(\boldsymbol{B}\right) - J_i N_i dS \\ P_{ij} &= -\int_S \nabla \times \left(N_i e_z\right)^T \left[\frac{\partial \boldsymbol{H}\left(\boldsymbol{B}\right)}{\partial \boldsymbol{B}} \right] \nabla \times \left(N_j e_z\right) dS \end{aligned} \tag{16}$$

where N_i is the shape function of the finite element method, i and j are node numbers.

The incremental reluctivity tensor $\partial \boldsymbol{H} / \partial \boldsymbol{B}$ is determined by differentiating the energy density w (8). Its expression is given by:

$$\frac{\partial \boldsymbol{H}(\boldsymbol{B})}{\partial \boldsymbol{B}} = \begin{bmatrix} \frac{\partial h_x}{\partial b_x} & \frac{\partial h_x}{\partial b_y} \\ \frac{\partial h_y}{\partial b_x} & \frac{\partial h_y}{\partial b_y} \end{bmatrix} = \begin{bmatrix} \frac{\partial^2 w}{\partial b_x^{\,2}} & \frac{\partial w}{\partial b_x \partial b_y} \\ \frac{\partial w}{\partial b_x \partial b_y} & \frac{\partial^2 w}{\partial b_y^{\,2}} \end{bmatrix} \tag{17}$$

The windings of three phases supply are modelled with six Dirichlet boundary conditions:

$$\begin{aligned} &\boldsymbol{A}_{d1} = 0 && \boldsymbol{A}_{d2} = -A_c(t) && \boldsymbol{A}_{d3} = A_b(t) - A_c(t) \\ &\boldsymbol{A}_{d4} = A_b(t) - A_a(t) - A_c(t) && \boldsymbol{A}_{d5} = A_b(t) - A_a(t) && \boldsymbol{A}_{d6} = -A_a(t) \end{aligned} \tag{18}$$

where $A_a(t)$, $A_b(t)$, and $A_c(t)$ corresponds to the three phases supply. They are determinated by:

$$A_a(t) = A_{\max}\cos(\omega t) \qquad A_b(t) = A_{\max}\cos(\omega t - 2\pi/3) \qquad A_c(t) = A_{\max}\cos(\omega t + 2\pi/3) \tag{19}$$

where $A_{\max}$ is the amplitude of the magnetic vector potential ($A_{\max}$=1.7 mT.m) and ω is the time pulsation corresponding to 50 Hz. One period is discretized into 200 time-steps.
Those conditions are imposed on the edges of the 6 legs (Figure 8a).

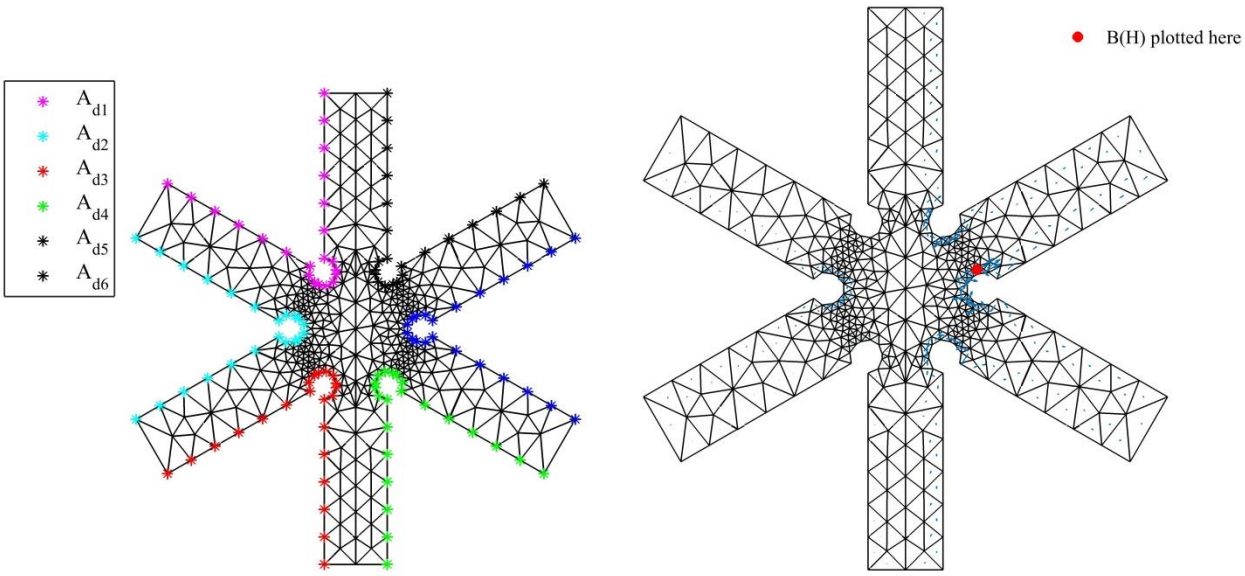

(a) Geometry and boundary conditions (b) Flux density vectors

Fig. 8. Representation of the rotational single sheet tester. The flux density vectors are plotted at the instant matching with two periods

In Figure 8.b, we can notice that the flux density is not as homogeneous as in isotropic material. The flux lines are mainly located in the edges of the rotational sheet tester. At the position indicated in Figure 8.b, the $\boldsymbol{B}(\boldsymbol{H})$curves are represented in Figure 9. We can first observe that the flux density is unidirectional in the legs of a rotational sheet tester. Then, for small amplitude of $\boldsymbol{B}$, the magnetic properties are isotropic as it was noticed in table II and section 4. Finally, the suggested model of magnetic anisotropy is suitable for its incorporation with finite element methods.

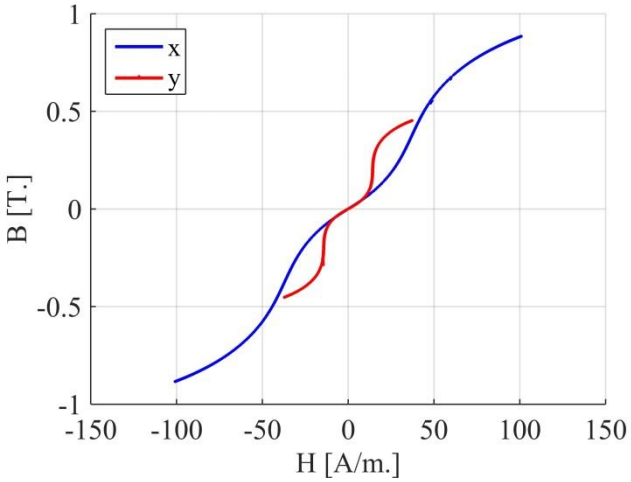

Fig. 9. Representation of the magnetic properties of both components $b_x(h_x)$ and $b_y(h_y)$ at an arbitrary location of the rotational sheet tester

6. Conclusion

The suggested model is based on an analytical formulation of the energy depending on the components of the magnetic flux density. This formulation is composed of 3 Gumbel distributions. Every functional parameters of energy density is formulated with only 4 parameters which are calculated by fitting the energy extracted from measurements. The components of the magnetic field are then deduced by differentiating the magnetic energy with respect to the components of the magnetic flux density. Hence, with this analytical formulation, the determination of **H** does not require any iterative process as it is usually the case with this energy method coupled with implicit function. Finally, the proposed model is validated by comparing the computation and the measurements of 9 **H** loci for non-oriented steel sheets at 10 Hz. The proposed analytical model shows good agreements with an average relative error of 22 %.

Besides, the suggested model is implemented into a finite element method for a rotational sheet tester. Its incorporation is relatively easy. In further work, it could be relevant to improve the measurement control in order to apply perfectly circular loci of the rotating flux density.

References

A. Belahcen, D. Singh, P. Rasilo, F. Martin, S. Ghalamestani, and L. Vandelvelde (2014), "Anisotropic and strain-dependent model of magnetostriction in electrical steel sheets", *in Conference on Electromagnetic Field Computation* – CEFC, Annecy, 2014

M. Belkasim (2008), "Identification of loss models from measurements of the magnetic properties of electrical steel sheets," Master's thesis, Helsinki University of Technology.

O. Bíró, S. Außerhofer, K. Preis, and Y. Chen (2010), "A modified elliptic model of anisotropy in nonlinear magnetic materials", *Compel*, vol. 29, no. 6, pp. 1482–1492.

R. Brent (1973), *Algorithms for Minimization without Derivatives*, Prentice-Hall.

S. Chikazumi (1997), *Physics of Ferromagnetism*. Oxford University Press.

K. Chwastek (2013), "Anisotropic properties of non-oriented steel sheets", *Electric Power Applications*, IET, vol. 7, no. 7, pp. 575–579.

B. D. Cullity and C. D. Graham (2008), *Introduction to Magnetic Materials*, 2nd Edition. Wiley-IEEE Press.

M. Enokizono and N. Soda, (1995), "Magnetic field analysis by finite element method using effective anisotropic field", *IEEE Trans. on Magnetics*, vol. 31, no. 3, pp. 1793–1796.

F. Fiorillo, R. Dupré, C. Appino, and A. M. Rietto, "Comprehensive model of magnetization curve hysteresis loops, and losses in any direction in grain-oriented Fe-Si", *IEEE Trans. on Magnetics*, vol. 38, no. 3, pp. 1467–1476, 2002.

K. Fujisaki, Y. Nemeto, and R. Hirayama (2004), "Electromagnetic steel solution in electromagnetic field technique", Tech. Rep. 89, Nippon Steel Technical Report.

E. Gumbel (1935), "Les valeurs extrêmes des distributions statistiques", *Annales de l'institut Henri Poincaré*, vol. 5, no. 2, pp. 115–158.

P. Handgruber, A. Stermecki, O. Bíró, V. Goričan, E. Dlala, and G. Ofner (2014), "Anisotropic generalization of vector preisach hysteresis models for non-oriented steels", *in Conference on Electromagnetic Field Computation* – CEFC, Annecy, 2014

S. Higuchi, T. Nakao, Y. Takahashi, T. Tokumasu, K. Fujiwara, and Y. Ishihara (2012), "Modeling of two-dimensional magnetic properties based on one-dimensional magnetic measurements", *IEEE Trans. on Magnetics*, vol. 48, pp. 3486–3489.

S. Higuchi, Y. Takahashi, T. Tokumasu, and K. Fujiwara (2014), "Comparison between modeling methods of 2-d magnetic properties in magnetic field analysis of synchronous machines", *IEEE Trans. on Magnetics*, vol. 50, no. 2, pp. 373–376.

A. Kedous-Lebouc (2006), *Matériaux magnétiques en génie électrique 1*. Lavoisier, Hermès sciences ed., Paris

G. Meunier (2008), *The Finite Element Method for Electromagnetic Modeling*. Wiley-ISTE.

L. Néel (1944), "Les lois de l'aimantation et de la subdivision en domaines élémentaires d'un monocristal de fer", *J. Phys. et Radium*, vol. 5, no. 11, pp. 241–251.

J. Osborn (1945), "Demagnetizing factors of general ellipsoid", Phys. Rev., vol. 67, pp. 351–357.

T. Péra, F. Ossart, and T. Waeckerle (1993a), "Field computation in non linear anisotropic sheets using coenergy model", *IEEE Trans. On Magnetics*, vol. 29, no. 6, pp. 2425–2427.

T. Péra, F. Ossart, and T. Waeckerle (1993b), "Numerical representing for anisotropic materials based on coenergy modeling", *J. Appl. Phys.*, vol. 73, no. 10, pp. 6784–6786.

P. Rasilo, E. Dlala, K. Fonteyn, J. Pippuri, A. Belahcen, and A. Arkkio (2011), "Model of laminated ferromagnetic cores for loss prediction in electrical machines", *Electric Power Applications*, IET, vol. 5, no. 7, pp. 580–588.

G. Shirkoohi and J. Liu (1994), "A finite element method for modelling of anisotropic grain-oriented steels", *IEEE Trans. on Magnetics*, vol. 30, no. 2, pp. 1078–1080.

P. Silvester and R. P. Gupta (1991), “Effective computational models for anisotropic soft b-h curves”, *IEEE Trans. On Magnetics*, vol. 27, no. 5, pp. 3804–3807.

R. Skomski (2008), *Simple Models of Magnetism*. Oxford University Press.

C. Vernescu-Spornic, A. Kedous-Lebouc, S. A. Spornic, and F. Ossart (2000), “Anisotropic and vector hysteresis model for magnetic materials application to a cubic textured NiFe sheet”, *Physica B: Condensed Matter*, vol. 275, no. 13, pp. 99 – 102.